



HAL
open science

Pressure Loss Modeling for Multi-Stage Obstacles in Pressurized Ducts

Guillaume Bon, Ludovic Chatellier, Yves Le Guer, Cécile Bellot, Xavier Casiot, Laurent David

► **To cite this version:**

Guillaume Bon, Ludovic Chatellier, Yves Le Guer, Cécile Bellot, Xavier Casiot, et al.. Pressure Loss Modeling for Multi-Stage Obstacles in Pressurized Ducts. *Energies*, 2024, 17 (14), pp.3505. 10.3390/en17143505 . hal-04863796

HAL Id: hal-04863796

<https://hal.science/hal-04863796v1>

Submitted on 4 Jan 2025

HAL is a multi-disciplinary open access archive for the deposit and dissemination of scientific research documents, whether they are published or not. The documents may come from teaching and research institutions in France or abroad, or from public or private research centers.





L'archive ouverte pluridisciplinaire **HAL**, est destinée au dépôt et à la diffusion de documents scientifiques de niveau recherche, publiés ou non, émanant des établissements d'enseignement et de recherche français ou étrangers, des laboratoires publics ou privés.



Distributed under a Creative Commons Attribution 4.0 International License

Article

Pressure Loss Modeling for Multi-Stage Obstacles in Pressurized Ducts

Guillaume Bon ^{1,2,*} , Ludovic Chatellier ² , Yves Le Guer ³ , Cécile Bellot ¹, Xavier Casiot ¹ and Laurent David ² 

¹ France Hydro Electricité, 75008 Paris, France

² Institut Pprime, Université de Poitiers, 86073 Poitiers, France

³ Laboratoire SIAME, Université de Pau et Pays de l'Adour, 64000 Pau, France

* Correspondence: guillaume.bon@univ-poitiers.fr

Abstract: Estimating singular pressure losses for multi-stage obstacles in pressurized hydraulic ducts is a challenging task. An experimental study was conducted in a closed-loop hydrodynamic tunnel to characterize the pressure losses of a system consisting of a porous fibrous foam placed in front of a bar rack. The pressure losses of different foam–rack configurations were measured over a range of inlet velocities in order to highlight the mutual influence of their characteristics on the flow. The interdependence between the two stages has been evidenced by both the experimental results and additional numerical simulations using RANS (Reynolds-Averaged Navier–Stokes Equations) simulations with a $k-\omega$ SST turbulent closure model. The pressure losses were first modeled using two approaches based on the assumption of either independence or full dependence between the stages. The respective advantages and limitations of these approaches led to an improved analytical formula that considers the transition of the flow from the porous foam to the bar rack. By taking into account an empirical transition factor, the proposed model improves the head loss prediction for all tested configurations, with an average relative error between the formula and experimental results less than that of the two simpler approaches. This study improves our understanding of global pressure losses in multi-stage systems that include a porous foam or other filtering or clogging media in front of bar racks.

Keywords: pressure loss association; experimental study; numerical simulation; bar rack clogging; analytical formula



Citation: Bon, G.; Chatellier, L.; Le Guer, Y.; Bellot, C.; Casiot, X.; David, L. Pressure Loss Modeling for Multi-Stage Obstacles in Pressurized Ducts. *Energies* **2024**, *17*, 3505. <https://doi.org/10.3390/en17143505>

Academic Editor: Artur Blaszczyk

Received: 24 June 2024

Revised: 12 July 2024

Accepted: 14 July 2024

Published: 17 July 2024



Copyright: © 2024 by the authors. Licensee MDPI, Basel, Switzerland. This article is an open access article distributed under the terms and conditions of the Creative Commons Attribution (CC BY) license (<https://creativecommons.org/licenses/by/4.0/>).

1. Introduction

Obstacles and rapid changes in flow can result in brutal head losses due to pressure, friction, detachment, or turbulence. Depending on the application, excessive head loss can be harmful, provoke cavitation, or alter the flow topology. It is therefore important to estimate it carefully in order to anticipate its effect. Comprehensive books, such as Id'lcik [1] and the Applied Fluid Dynamics Handbook by Blevins [2], focus on the estimation of the many obstacles in pipes and free channel flow. However, estimating head losses becomes challenging for complex systems with multiple obstacle stages or layers that create intricate flow features. In the case of elements separated by long distances, head losses can be considered independent of each other. However, for successive or narrow stages, it is no longer possible to consider them as independent.

Multi-stage obstructions with independent stages in a hydraulic system allow the intrinsic loss of each stage to be directly related. In hydraulic pipe circuits, there are some simple tools available to determine the relationship between losses. Since the losses are independent, they can be considered in parallel or in series, by analogy with electrical circuits. Simple regular or singular head losses in pipes can then be associated and calculated directly using this analogy (Rodriguez [3]).

For systems with dependent regular and singular head losses, the applicability of electrical equivalence is limited. Estimation of pressure losses in such systems with stage

dissociation is still uncommon and only a few studies have considered the inter-stage dependency issues. In some applications, such as gas or water turbines, it is important to control the pressure in pressurized systems to improve efficiency and prevent cavitation. To achieve that, multi-stage obstacles can be implemented in the piping to regulate the pressure. Filtration, particularly air filtration, uses multi-layer filters to improve filtration performance. Flow strainers and bar racks are widely used devices that can generate significant head losses. The interaction between the various components of a bar rack has been investigated in the absence of clogging effects (Lemkecher et al. [4]). They are indeed also susceptible to clogging, which can be considered as an additional layer, or stage, that exacerbates pressure drop or water level loss.

To control pressurized systems, series of perforated plates can be implemented in pipes. The velocity profile of such plates has been extensively studied (Xiong et al. [5]). In their analysis, Cho and Rhee [6] investigated the effect of the distance between two identical or similar stages of perforated plates on the flow. La Rosa et al. [7,8] investigated the effect of the spacing between plates on the pressure drop in a similar application using two stages of flat perforated plates. For a small spacing between plates, the pressure loss is different from the simple addition of the pressure drops of the two plates considered independently. Depending on the orientation of the two stages and the distance between them, the total pressure loss may be higher or lower than the simple addition. Many parameters interact on the pressure loss of association of perforated plates (Qian et al. [9], Haimin et al. [10]), which complicates the determination of the simple formulation. This dependency between the stages is a crucial point for associating pressure losses, especially since the flow disturbance created by the first stage is rarely dissipated when the second stage is introduced.

In some applications, the system may have many stages. For example, in certain circumstances, the filtration of a mask may require the use of a multi-layered filtration membrane. Kang et al. [11] analyzed the effect of using multiple layers on filtration performance and pressure drop. They used a series of large-hole nylon grids and nanofiltration membranes and found that adding layers does not simply result in a sum of each layer's pressure drop. Adding layers increases the filtration capacity, while the effect on the pressure drop of the nylon grid was expected to be negligible compared to that of the nanofiltration membrane, so the layers were assumed to be identical. The impact of multi-layer filtration on pressure drop and filter efficiency was also investigated by Agui et al. [12] for a cabin ventilation system on the ISS (International Space Station). The challenging interrelationship between the stages was highlighted.

The successive stages can be very different in nature. In the current study, a porous foam surface is added in front of a bar rack in order to mimic integral clogging. This type of combination is often observed, for example, in clogged air filtration systems, for bar racks or strainers. Pressure or head losses due to clogging problems in bar racks or strainers for hydraulic systems and hydroelectric power plants (HPPs) can be very high, reducing production and causing structural damage. In their study, Walczak et al. [13] analyzed the force exerted on the bar rack with an additional porous foam surface representing clogging by leaf or branches. Their findings demonstrated the significant impact of clogging on the force applied to the bar rack and to the supports. The clogging appears mainly from leaves, small tree branches, and artificial debris (Walczak [14] and Yan et al. [15]) but also due to larger debris like tree trunks (Schalko et al. [16,17], and Zayed and Farouk [18]). Other clogging issues, such as ice clogging during cold seasons, may also have an impact on the production and security of the power plant (Walczak et al. [19] and Gebre et al. [20]). Estimating the exact impact of clogged surfaces remains a challenging task. Some studies have focused on developing formulae for the losses generated by the clean bar rack, but few of them have considered additional clogging stages. In the first instance, a specific factor to account for clogging can be added to the clean bar rack formulae. The first approach is to multiply the formula directly by a factor dedicated to clogging (Meusburger et al. [21], Raynal et al. [22]). This assumes a direct relationship between the clogging

surface and the bar rack, without explaining exactly how it occurs. The complexity of anticipating all clogging configurations with this approach was noted in these studies. A second approach is to add a clogging loss formula directly to the clean bar rack formula. Hribernik [23] separates the head losses into an addition of a clean bar rack head loss and an additional clogging head loss, based on the assumption of independence between the two stages. This is achieved by simply adding the two individual losses. Yan et al. [15] introduced a new method based on energy momentum to estimate the total losses using the flow deviation due to partial clogging on the bar rack. For filtration and trainer system, clogging may be very damaging with an increase in pressure loss and permeability of the system (Dziubak [24]). The clogging surface can be considered as a porous fibrous foam (Violeau et al. [25]), especially for strainer and filtration applications. The real relationship between the porosity, porous foam thickness, and the pressure drop has been an important focus of studies considering the complexity of characterizing this phenomenon (Grahn et al. [26], Sotoodeh [27]). The need to control the pressure drop for the safety of pumping systems, such as those used in nuclear applications, is highlighted by Grahn et al. [26]. They developed a formulation based on a Darcy–Forchheimer equation to account for the pressure drop due to obstructed foam volume.

The present study investigates experimentally a fibrous porous medium placed at the front of a bar rack to determine an analytical formula predicting the pressure losses of this specific assembly. Such an assembly directly addresses the clogging problems encountered in bar rack and filtration systems, as porous material filtratum requires an additional stage to fix it in filtration systems. An experimental study is performed in a closed-loop hydraulic tunnel to determine the pressure losses of the system. The dependence between the two stages is studied using different approaches. A combination of experimental and numerical studies led to the development of a new analytical formula based on a novel approach.

2. Model and Methods

2.1. Experimental Setup

The experiments have been conducted using a hydrodynamic tunnel. The closed-loop has a total length of 20 m and a $230 \times 230 \text{ mm}^2$ test section with a length of 700 mm (refer to Figure 1). In the measurement section, the flow can reach a velocity (v) of $6 \text{ m}\cdot\text{s}^{-1}$. A sheet of porous material has been placed in front of a bar rack system consisting of a series of rectangular profiles in the center of the measurement volume (see Figure 2).

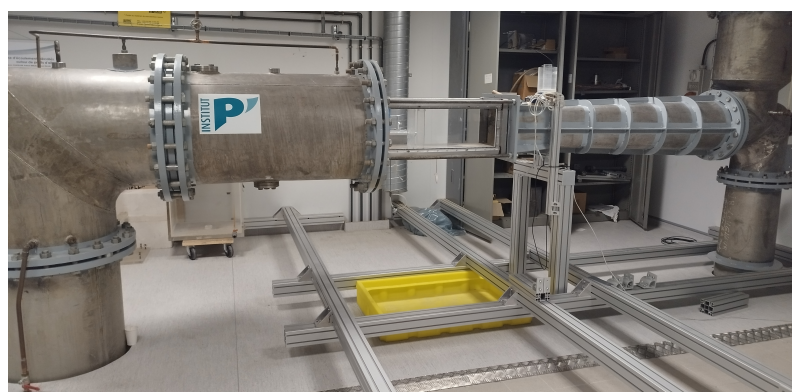


Figure 1. Upper part of the hydrodynamic tunnel used to conduct the experiments.

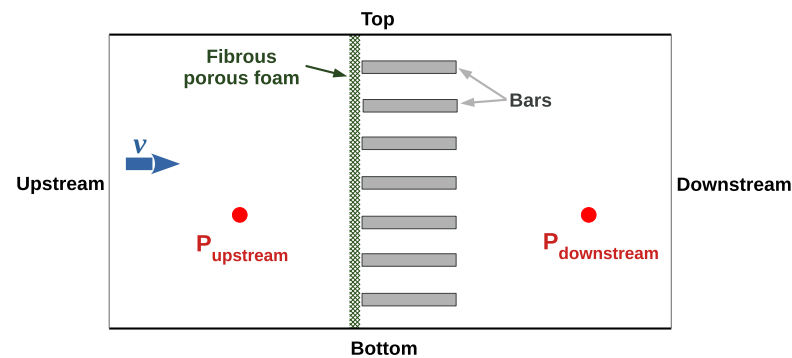


Figure 2. Rectangular measurement section displaying the multi-stage obstruction system and the different sensors in a front view. The flow is moving from the left to the right.

The porous fibrous material consisting of interwoven filaments is supplied by MAPA-SPONTEX (MAPA-SPONTEX IBERICA, Barcelona, Spain). Two different porous fibrous surface foams were tested, including the surfaces named ‘TV’ and ‘TV Extra’. ‘TV’ has a surface density of $530 \text{ g}\cdot\text{m}^{-2}$ for a surface obstruction of 72%, while TV EXTRA has a surface density of $670 \text{ g}\cdot\text{m}^{-2}$ for a surface obstruction (o_c) of 78%. The thickness of the two porous volumes (Δx) is approximately 8 mm. The characteristics (permeability K and Ergün α constants) needed to estimate the pressure losses induced by these porous foam are initially unknown (see Equation (3)). The study is therefore also dedicated to the determination of these coefficients, while investigating the relationship between the pressure losses of each stage. These fibrous materials represent clogging caused by leaves, tree branches, and aquatic plants due to their small thickness and high obstruction ratio.

The bar rack consists of series of bars with a width (b) of 5 mm and a depth (p) of 40 mm. The spacing between the bars (e) can vary from 10 mm to 24 mm to modify the obstruction of the bar rack (o_b), as explained in Equation (1).

$$o_b = \frac{b}{e + b} \quad (1)$$

where o_b is the bar rack obstruction ratio [-], b is the bar width [m], and e is the spacing between bars [m].

Table 1 shows the different bar rack configurations. The different spacings allowed us to determine the interaction between the bar rack and the porous foam, and to determine the characteristics of the porous fibrous foam. To avoid cavitation at the tunnel pump, the inlet velocity (v) is varied from 0 to a maximum of $1.5 \text{ m}\cdot\text{s}^{-1}$ depending on the pressure losses induced by each configuration.

Table 1. Bar rack configurations tested in the hydrodynamic channel with different porous foam. This includes the bar rack obstruction o_b .

Configurations	Spacings e [mm]	Bar Numbers	o_b [%]
1	10	15	33
2	15	11	25
3	24	07	17

2.2. Measurements

The hydrodynamic tunnel allows accurate calculation of pressure losses through the multi-stage system of the bar rack and porous fibrous foam. The differential pressure (ΔP) between upstream and downstream of the system is measured using a pressure sensor with a range of either 50 or 250 mbar (Sensortech (new name, First Sensor, Berlin, Germany) 26-PC wet-wet), depending on the measured pressure difference. The positions of the pressure points are shown in Figure 2. The upstream pressure point is positioned 100 mm

from the bars and the downstream pressure point 200 mm from the bars. The velocity is measured using a pitot tube and a differential pressure sensor with a range of 50 mbar (refer to Equation (2)).

$$\Delta P = \frac{1}{2} \rho v^2 \quad (2)$$

where ΔP is the pressure drop [Pa], v the inlet velocity [$\text{m}\cdot\text{s}^{-1}$], and ρ the water density [$\text{kg}\cdot\text{m}^{-3}$].

There are several uncertainties in the measurements, mainly from the sensors. The pressure sensor has been calibrated and has an inherent uncertainty of 0.2% of the maximum pressure. It gives an uncertainty of 0.1 mbar for the 50 mbar measurement and 0.5 mbar for the 250 mbar measurement. Raynal [28] checked the position of the pressure sensors. The uncertainty of the pitot measurements depends on the pressure sensor's uncertainty, the resulting angle of the pitot tube (less than 1 degree), and the presence of air bubbles in the tube. Each measurement was confirmed to be bubble-free and the resulting angle was found to be negligible. For each configuration, the standard deviation of the datasets was calculated to be used in the uncertainty propagation calculation in order to ensure a 95 percent confidence level. The general uncertainties have been estimated to be approximately 6.5% of the measured pressures on average. Some configurations were measured twice to ensure repeatability and to check the effect of the time of data acquisition on the results. While special cases with specific velocity and pressure losses may be affected, the majority of measurements have low general uncertainties.

2.3. Numerical Support for Coefficient Readjustment

Computational Fluid Dynamics (CFD) simulations have been used to better understand the flow passing through the system. Determining the relationship between pressure losses and bar spacing is challenging using only experimental studies and without detailed knowledge of the porous fibrous material characteristics. By matching experimental and simulation results, it is possible to determine the characteristics of the porous media and its interaction with the bar rack. The OpenFOAM v2112 computational library is used for these simulations. The library solves the Navier–Stokes equations using the finite volume method. As the flow is turbulent, the Reynolds-averaged Navier–Stokes (RANS) equation is calculated using a turbulent closure model. The $k-\omega$ SST turbulent model is chosen for its suitability for such simulations (Raynal et al. [29]). This model is well suited for flows with abrupt changes and for flow near wall surfaces, with the added advantage of being able to transition to a $k-\epsilon$ model in the free stream. A 3D domain is created to represent the measurement chamber of the experimental vein (Figure 3), whose boundary conditions are summarized in Table 2. Wall functions are implemented for the turbulent kinetic energy (k), the turbulent viscosity (ν_t), and the turbulent specific dissipation rate (ω), according to a small to high dimensionless wall distance (y^+) value in front of the bars.

The simpleFoam solver is used with the pressure–velocity coupling performed using the Semi-Implicit Linked Equations algorithm. The turbulence intensity (TI) is set to 5% at the inlet. The initial mesh is structured and then refined close to the bars. The number of cells depends on the configuration, and in particular, on the bar spacing to ensure an accurate flow between the bars. The characteristics of the simulation are shown in Table 3.

The porous fibrous foam stage is implemented as a volume in front of the bar rack using the Darcy–Forchheimer equation, Equation (3), for cells located in the porous material volume. The Darcy–Forchheimer equation allows the permeability (K) and the Ergün coefficient (α) to be calculated.

$$\frac{\Delta P}{\Delta x} = \frac{\mu}{K} v + \frac{\alpha}{\sqrt{K}} \rho v^2 \quad (3)$$

where Δx is the thickness of the porous foam [m], μ is the dynamic viscosity [Pa·s], K is the permeability coefficient [m²], v is the inlet normal velocity [m·s⁻¹], and α is the Ergün coefficient [-].

The mesh convergence was tested to validate the final mesh based on the convergence of the pressure drop of the system and the velocity profile on a vertical line in the porous foam, which is represented by the red line in Figure 3. A variety of structured meshes were developed, including those with 0.17×10^6 , 4.5×10^6 , 11×10^6 , 21×10^6 , and 30×10^6 cells. The velocity profiles in the x -direction (v_x) and the y -direction (v_y) along the specified line have been plotted in Figure 4. The velocity and pressure drop convergence has been analyzed to identify the optimal mesh (grid 4, with 21×10^6 cells), which has been selected for simulations.

Table 2. Boundary conditions imposed for the numerical simulations of the tested configurations (with TI the turbulence intensity).

	Inlet	Sides	Outlet	Bars
velocity	Fixed velocity	No slip	Zero gradient	No slip
pressure	Zero gradient	Zero gradient	Fixed pressure	Zero gradient
TI	Fixed TI	Wall function	Zero gradient	Wall function

The bar Reynolds number Re_b is used to predict flow patterns for such systems and it is defined in Equation (4).

$$Re_b = \frac{vb}{\nu} \quad (4)$$

where Re_b is the Reynolds number [-] and ν is the kinetic viscosity [m²·s⁻¹].

Table 3. Characteristics of the numerical simulations, such as the domain size, cell size, and inlet velocity.

v	Re_b Equation (4) [-]	Domain (x,y,z) [m]	Cell Size (x,y,z) [m]	$Y+_{bars}$ [-]
0–0.8	0–6400	(0.5,0.23,0.23)	$(0.9,0.7,0.7) \times e^{-3}$	0.7–25

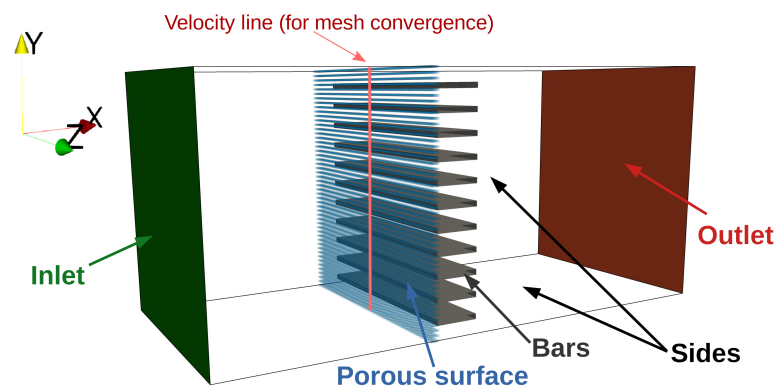


Figure 3. Numerical domain with the named boundaries and simulated porous volume.

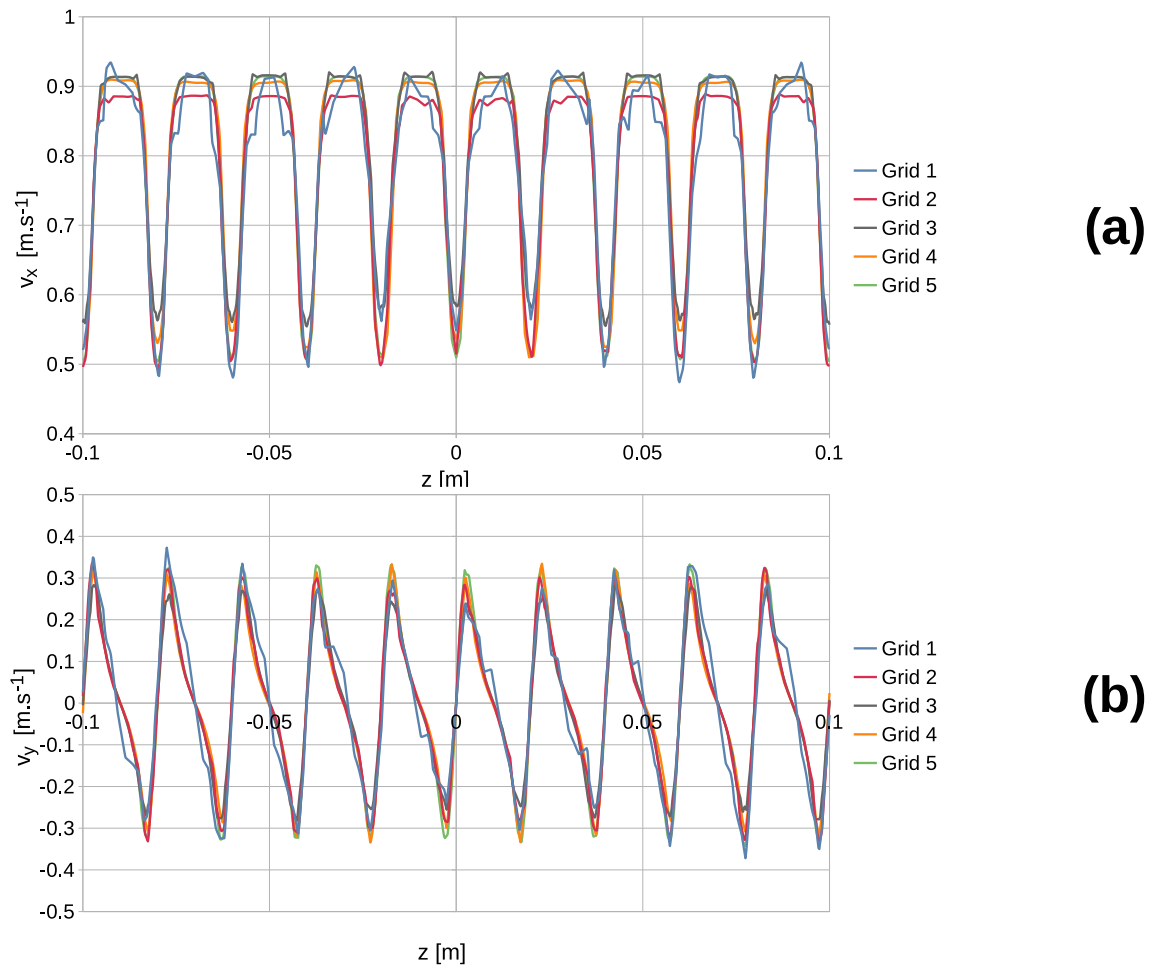


Figure 4. Grid convergence for the velocity components v_x in (a) and v_y in (b) on a line in the y -direction on the porous foam. Grids 1, 2, 3, 4, and 5 have, respectively, 0.17×10^6 , 4.5×10^6 , 11×10^6 , 21×10^6 , and 30×10^6 cells.

3. Results

3.1. Head Loss Evolution for the Grid

In order to determine the interaction between the porous fibrous foam and the bar rack, configurations without the porous media were used to determine the head loss coefficient (ζ) of the bar rack alone. Raynal [28] produced similar experiments in the same closed-loop tunnel and defined an analytical formula to evaluate the pressure loss coefficient of different bar racks. The configurations are tested again in order to validate the Raynal's formulation and to start from a clean bar rack pressure loss calculation with the same external parameters as the clogging bar rack experiments. The pressure loss of the three grid (bar rack) configurations was measured for velocities ranging from 0 to $1.5 \text{ m}\cdot\text{s}^{-1}$. The pressure loss versus the dynamic pressure, plotted in Figure 5, shows the linear relationship between the two variables. The slope is directly related with the pressure loss coefficient (ζ) (see Equation (5)).

$$\zeta = \frac{\Delta P}{\frac{1}{2}\rho v^2} \quad (5)$$

where ζ is the dimensionless pressure loss coefficient [-].

The pressure loss coefficients of each configuration are summarized in Table 4, and are in accordance with the formula developed for pressurized conditions by Raynal [28] (Equation (6)). The power factor for the obstruction part of the formula is 1.5. However,

the head loss coefficient formula of Raynal et al. [30] in the context of an inclined bar rack in free surface flow has a power factor of 1.65 for the obstruction part, as presented in Equation (7). It is possible to employ this second formula for an angle inclination of 90° and a form factor A_i of 2.5. It should be noted that the form coefficient of 2.5 is distinct from the form coefficient of 3.85, which was defined by Raynal for rectangular profiles in free surface flow. In free surface flow, in addition to the drag effect, there is also a spray and waves effect, and a ventilation effect due to the cavity downstream of the bar rack. These two formulae remain similar with comparable results (see Table 4). The second formula (Equation (7)) yields slightly better results, with a mean relative error of 8.6% in comparison to the Raynal formula in pressurized conditions, which exhibits a mean relative error of 9.4%. For a given bar width b , the head loss coefficient increases as the bar spacing decreases. This is due to the reduction in the free flow section caused by the increase in the bar rack obstruction o_b .

$$\zeta_{Raynal} = 2.04 \left(\frac{o_b}{1 - o_b} \right)^{1.5} = 2.04 \left(\frac{b}{e} \right)^{1.5} \tag{6}$$

$$\zeta_{Raynal,2} = A_i \left(\frac{o_b}{1 - o_b} \right)^{1.65} \sin^2(\beta) \tag{7}$$

where A_i is the bar form coefficient [-] and β is the inclination angle of the bar rack [°].

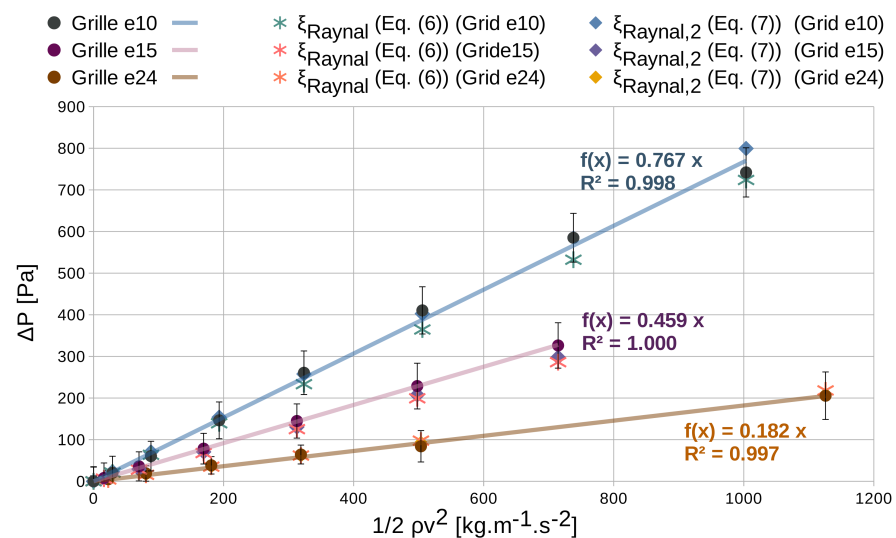


Figure 5. Global pressure loss evolution as a function of the dynamic pressure for the different bar racks without the porous foam volume ($e10$, $e15$, and $e24$ being the bar racks with 10, 15, and 24 mm spacing, respectively).

Table 4. Experimental head loss coefficient of the bar racks alone measured experimentally and calculated using the Raynal formula in Equation (6).

Case	Bar Spacing e [mm]	$\zeta_{measured}$ [-]	ζ_{Raynal} Equation (6) [-]	$\zeta_{Raynal,2}$ Equation (7) [-]
e10	10	0.767 ± 0.06	0.721	0.721
e15	15	0.459 ± 0.08	0.393	0.401
e24	24	0.182 ± 0.03	0.194	0.194

3.2. Head Loss Evolution for Both Porous Foams

The characteristics of the porous fibrous volume and the relationship between the two stages are analyzed by measuring the pressure losses of the global system. The pressure losses have been measured for configurations with the two different fibrous foam surfaces

and by varying the spacing between bars and the inlet velocity. The evolution of the global pressure loss as a function of the velocity can be considered as a polynomial with only linear and quadratic terms, as shown in Figure 6 for a bar rack with a spacing of 15 mm and for both of the two surfaces. It is in accordance with the Darcy–Forchheimer formula. The v^2 term is the dominant factor for velocities above $0.06 \text{ m}\cdot\text{s}^{-1}$ and $0.013 \text{ m}\cdot\text{s}^{-1}$ threshold, respectively, for the porous foams ‘TV EXTRA’ and ‘TV’. For higher velocity, the term associated with v is negligible compared to the part of v^2 , and the porous surface is treated as a flat surface with a pressure loss dependent only on v^2 . The pressure losses of the ‘TV EXTRA’ are higher than those of ‘TV’ according to the density difference between the two volumes.

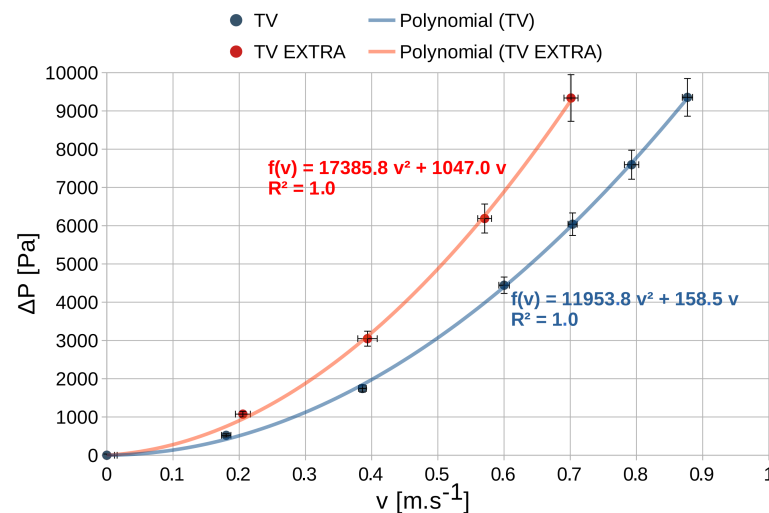


Figure 6. Evolution of the pressure loss as a function of the velocity for a distance of 15 mm between the bars and the two porous foam volumes.

3.3. Head Loss Combination

The resulting pressure loss (ΔP_{foam}) is determined by subtracting the initial pressure drop of the bar rack alone (ΔP_{grid}) from the total pressure difference of the tested configuration (ΔP). The resulting pressure ΔP_{foam} represents the pressure loss across the porous fibrous surface for a given downstream bar rack.

Two approaches can be considered in which the bar rack and foam are associated as elements in either series or interlaced arrangement (Figure 7). Considering the rack and foam as two successive stages yields the simpler approach of two elements in series; this is obtained and consists of a simple addition of two terms (see Equation (8)).

$$\Delta P = \Delta P_{foam}(v) + \Delta P_{grid}(v) \quad (8)$$

where ΔP_{foam} is the resulting pressure drop [Pa] and ΔP_{grid} is the pressure drop of the grid alone [Pa].

As the porous media and the grid are contiguous, the simple electrical series analogue approach may not be the best approach, as it neglects the mutual influence of the two stages, as shown by La Rosa et al. [8]. It is essential to have a clear understanding of how head losses are related to such a system. The bar rack may have an effect on the flow through the porous media.

A second approach is to consider that the flow through the porous media is equivalent to the flow velocity seen between the bars (see Figure 7b). The flow velocity between the bars is defined as an accelerated velocity, denoted (v_a), as shown in Equation (9). The equation for this interlaced approach is given in Equation (10) and may be equivalent to the multiplication of two factors. This approach is typically correct when an additional flat surface obstruction is placed in front of the grid. However, for a volume such as the porous

foam volumes studied in this case, the flow through the porous foam may be a transient flow and a combination of the simple and interlaced approaches may be required.

$$v_a = v \times \frac{1}{1 - o_b} \quad (9)$$

where v_a is the accelerated velocity between bars [$\text{m}\cdot\text{s}^{-1}$].

$$\Delta P = \Delta P_{foam}(v_a) + \Delta P_{grid}(v) \sim \Delta P_{grid}(v) \times (1 + K_{foam}) \quad (10)$$

where K_{foam} is a coefficient representing the foam losses in front of the bar rack [-].

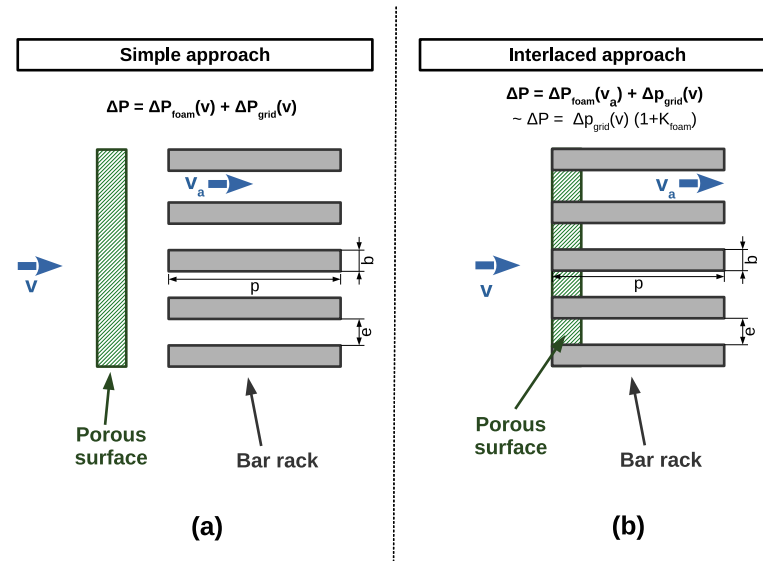


Figure 7. Different approaches for pressure association with a simple series model in (a) and a second approach with an interlaced model in (b).

To compare the two approaches, the resulting pressure loss versus, respectively, the inlet velocity v for the simple approach and the increased velocity between bars v_a for the interlaced approach, was analyzed for the different bar spacings. Figure 8 illustrates this evolution for the TV porous media and the simple series approach case. The resulting pressure loss as a function of the inlet velocity is dependent on the bar spacing for this approach. The permeability and Ergün coefficients calculated with the different configurations will not be identical, but will depend on the bar rack spacing. Consequently, the separation of the two stages is inaccurate in this case and the pressure loss $\Delta P_{foam}(v)$ does not characterize the independent loss generated by the porous media.

Figure 9 illustrates the interlaced approach by showing the $\Delta P_{foam}(v_a)$ evolution based on the accelerated velocity. The resulting pressure is here practically independent of the bar spacing. The $\Delta P_{foam}(v_a)$ then depends only on the properties of the porous media. The permeability and the Ergün coefficient no longer depend on the bar rack configuration. The interlaced approach better represents the behavior of the global system and validates the assumption that the flow velocity passing through the porous media is influenced by the induction zone just upstream of the bar rack. However, the independence of the pressure loss from the bar rack spacing may not be sufficient to understand the real relationship between the two stages. In fact, the characteristics of the porous foam are not known and $\Delta P_{foam}(v_a)$ may not perfectly characterize the media.

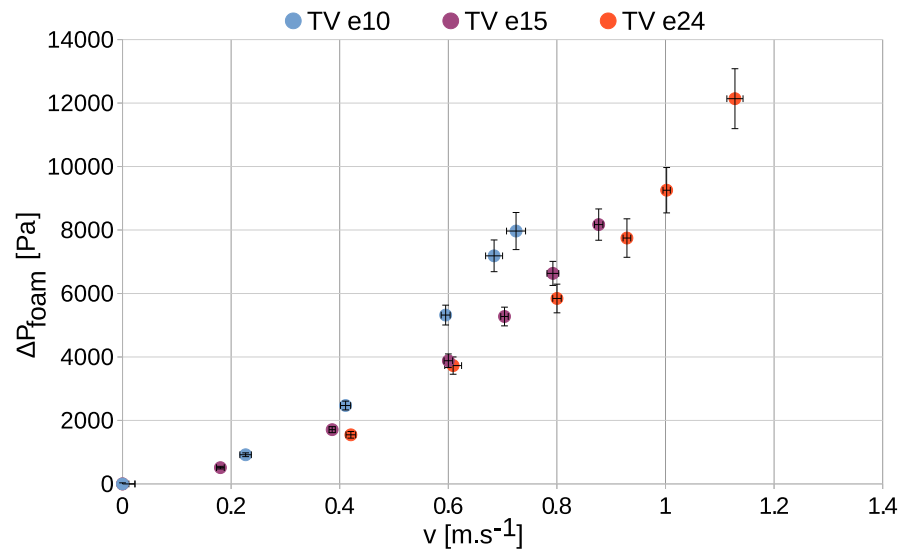


Figure 8. Resulting pressure loss, substituting the pressure drop of the clean bar rack, as a function of the inlet velocity for the 'TV' foam and different bar spacings (simple approach).

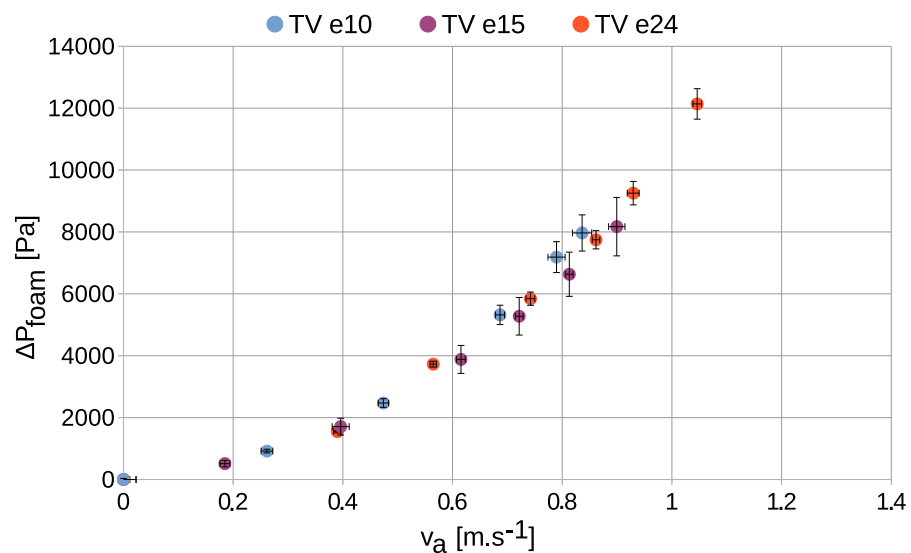


Figure 9. Resulting pressure loss, substituting the pressure drop of the clean bar rack, as a function of the velocity between bars for the 'TV' foam and different bar spacings (interlaced approach).

3.4. Fibrous Porous Foam Characterization

Since the porous media have a finite thickness, the second approach relies on the assumption of a uniformly accelerated flow and is not entirely accurate. The velocity of the flow within the foam is not homogeneously equal to the velocity between the bars, but rather in a transition phase from the inlet velocity (v) to the increased velocity between the bars (v_a). The experimental configurations were modelled and simulated using CFD simulations to understand the transition phase and to determine the characteristics of the porous foam by matching the experimental and simulation results. The initial permeability and Ergün coefficients of the porous foam were calculated using the interlaced approach. The coefficients have been adjusted, using a unique modification factor (f_t) for all configurations, to match both experimental and numerical results. This factor represents the transitional flow effect due to porous foam thickness and illustrates that the real behavior is between the simple series and interlaced approach. The f_t factor is assumed to depend only on the thickness and is determined as 0.82 for all porous fibrous surfaces tested here. Figure 10 shows a section of the computational domain with

the ‘TV’ porous media represented by the pink rectangle and a bar rack with a 15 mm spacing. The dimensionless longitudinal velocity, shown in Figure 10a, demonstrates the transitional flow in the porous foam volume and shows the importance of adding the additional f_t factor to the velocity across the porous foam. Figure 10b illustrates the pressure distribution within the domain and shows the influence of the bar rack on the pressure loss across the porous foam. The good results with these coefficients for the experimental domain do not prove that they are physical and applicable outside the tested range. This determination was important to validate the formulation of the association of pressure losses of a combined system, and it highlighted the need for an improved interlaced approach.

The characteristics of the porous surfaces have been defined (see Table 5). Figures 11 and 12 show the comparison between simulations and experiments for the total pressure difference ΔP for the global system depending on the inlet velocity for the porous fibrous foam ‘TV’ and ‘TV Extra’, respectively. For this permeability and Ergün coefficient, the simulation and experimental results are very close with a mean relative error of 6.3% for the ‘TV’ foam and 5.4% for the ‘TV Extra’ foam, confirming the identified characteristics. There is some difference for the bar rack with 10 mm spacing at the highest velocities, which can be explained by the technical limitations of the experimental tunnel. The pressure difference at these points is very high and some cavitation occurred at the pump, causing the change in pressure drop.

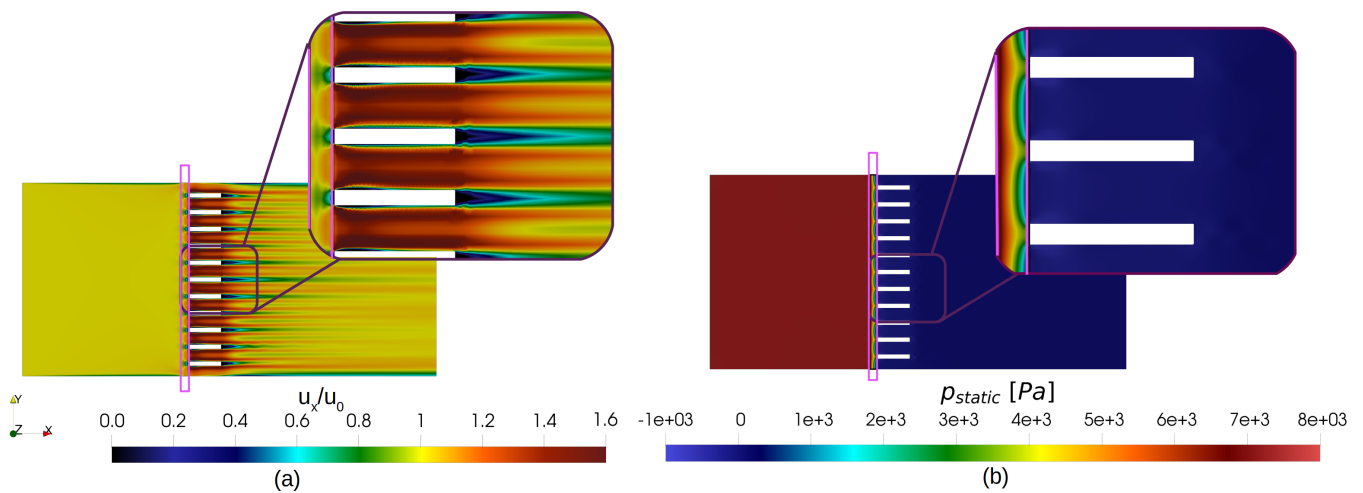


Figure 10. Non-dimensional longitudinal velocity (u_x/u_0) in (a) and the static pressure in (b) for the simulation with the porous media ‘TV’ and a grid of 15 mm bar spacing.

Table 5. Characteristics of the porous surfaces determined thanks to experiments and corrected by numerical simulations.

Porous Foam	TV	TV Extra
Permeability K [m^2]	$1.282 \times 10^{-8} \pm 1.4 \times 10^{-9}$	$8.126 \times 10^{-9} \pm 1.0 \times 10^{-9}$
Ergün α [-]	0.122 ± 0.020	0.150 ± 0.024

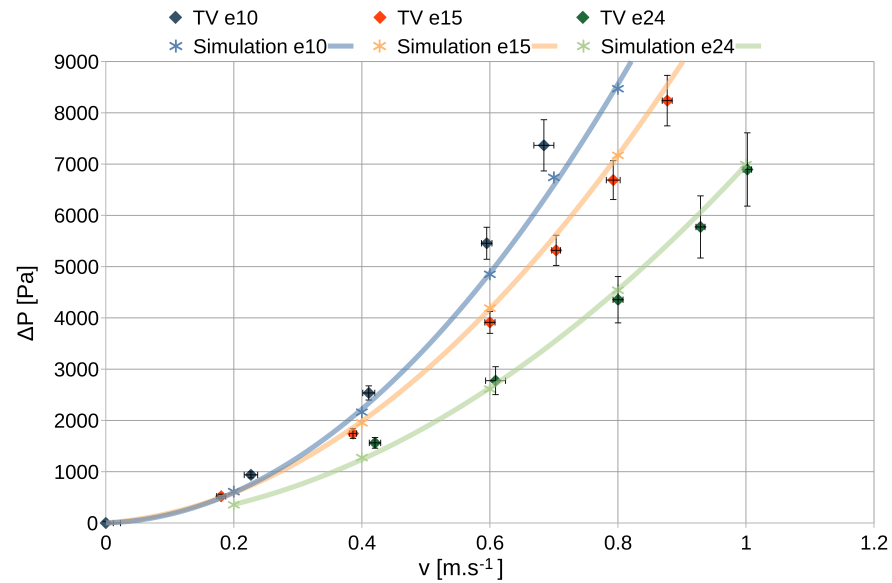


Figure 11. Total pressure drop of the system as a function of the inlet velocity from experiments and simulations for the ‘TV’ foam.

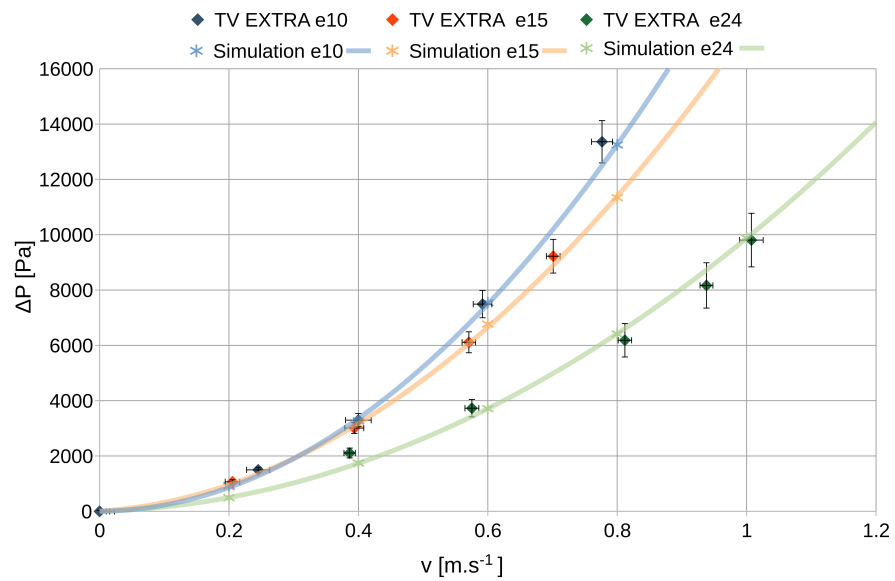


Figure 12. Total pressure drop of the system as a function of the inlet velocity from experiments and simulations for the ‘TV Extra’ foam.

3.5. Improvement of Interlaced Approach

It is possible to define an analytical formula that account for the f_t factor. The velocity through the porous foam surface is defined as a transition flow velocity, denoted as v_t , which depends on the thickness factor f_t (see Equation (11)). The new approach is shown in Figure 13 and the corresponding analytical formula is determined using this new velocity and is shown in Equation (12). The formula is a simple association of the bar rack loss and clogging loss adjusted by the thickness factor and the the bar rack obstruction.

$$v_t = f_t \frac{v}{1 - o_b} \tag{11}$$

where f_t is the thickness factor [-] and v_t the corresponding transitional velocity [m·s⁻¹].

$$\Delta P = \Delta x \left(\frac{\mu}{k} v_t + \frac{\alpha}{\sqrt{k}} \rho v_t^2 \right) + \Delta P_{grid}(v) \quad (12)$$

The comparison between the experimental results and the analytical formula (see Figures 14 and 15) confirms the accuracy of the model (Equation (12)) and the need to adjust the velocity through the porous media for such configurations. The new approach to associating pressure losses for such multi-stage systems, based on simple physical assumptions, gives accurate results for the tested configurations.

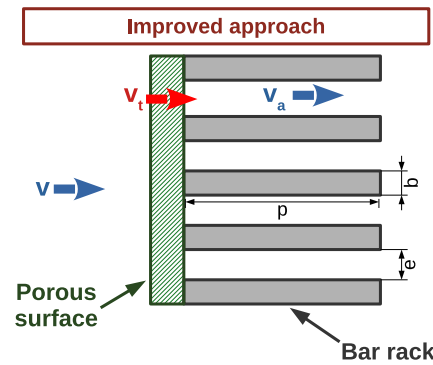


Figure 13. Improved approach taking into account the porous foam surface directly in front of the bar rack using a transition velocity v_t .

The final formulation explained in Equation (12) can be validated by comparing the series and interlaced approaches, and the final formula with the experimental measurements for the same velocities. For a bar spacing of 24 mm, the difference between the final formula and the series approach is negligible. In such cases, the flow in the porous foam is practically independent of the bar rack, as shown in Figure 15c. For bar spacings of 10 mm and 15 mm, this assumption is no longer valid and the advantages of using the final formula are highlighted, as shown in Figure 15a,b. Figure 14 compares the experimental results with the final formula for all bar rack spacings and the ‘TV Extra’ porous foam surface. The formula provides an accurate estimation of the global pressure losses, exhibiting good behavior with respect to bar rack spacing and inlet velocity. The final formula has a relative mean error E_{mean} (see Equation (13)) of approximately 6.3%, as shown in Table 6. This is significantly better than both the series approach and the interlaced approach. The series approach produces fewer errors than the interlaced approach. However, the interlaced approach is more effective for small bar spacing (see Figure 15a) because the obstruction of the bar rack is more intrusive for the flow in the porous foam. The final formula appears to represent more accurately the pressure drop for all configurations with a small relative error.

$$E_{mean} = \frac{1}{N} \sum_{i=1}^N \frac{|\Delta P_{exp,i} - \Delta P_{model,i}|}{\Delta P_{exp,i}} \quad (13)$$

where E_{mean} is the average relative error [%], N is the number of tested configurations [-], i is the tested configuration number i , and [-] and ΔP_{exp} are, respectively, the experimental and modeled pressure drop [Pa].

$$E_{max} = \max_{\{N\}} \left(\frac{|\Delta P_{exp,i} - \Delta P_{model,i}|}{\Delta P_{exp,i}} \right) \quad (14)$$

where E_{max} is the maximum relative error [%].

Table 6. Mean and maximum relative errors on both porous foam and three bar spacings for the three different approaches.

	Series Approach	Real Case	Interlaced Approach
E_{mean} [%] Equation (13)	14.7	6.3	41.6
E_{max} [%] Equation (14)	39.0	16.6	75.8

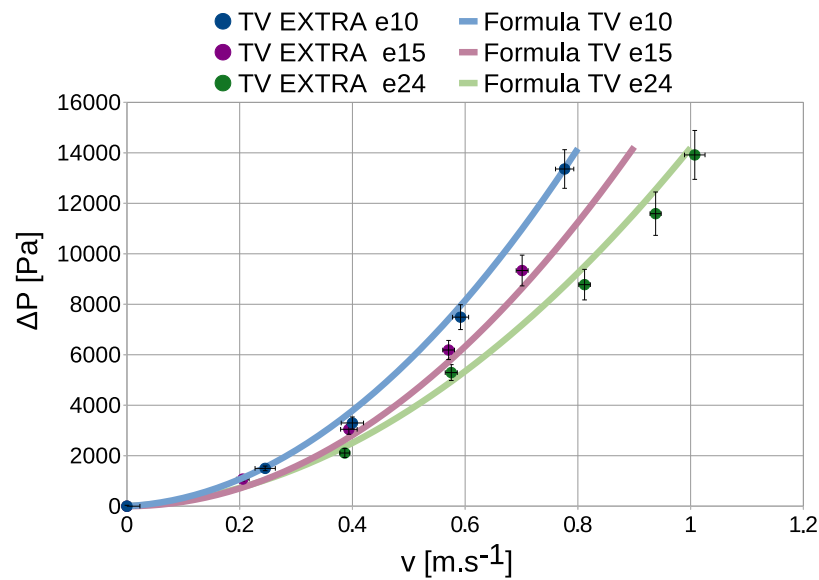
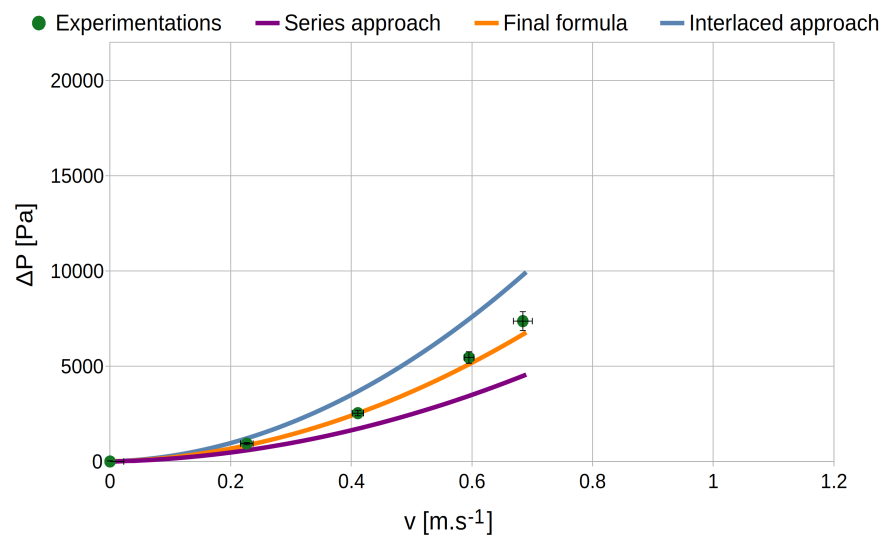
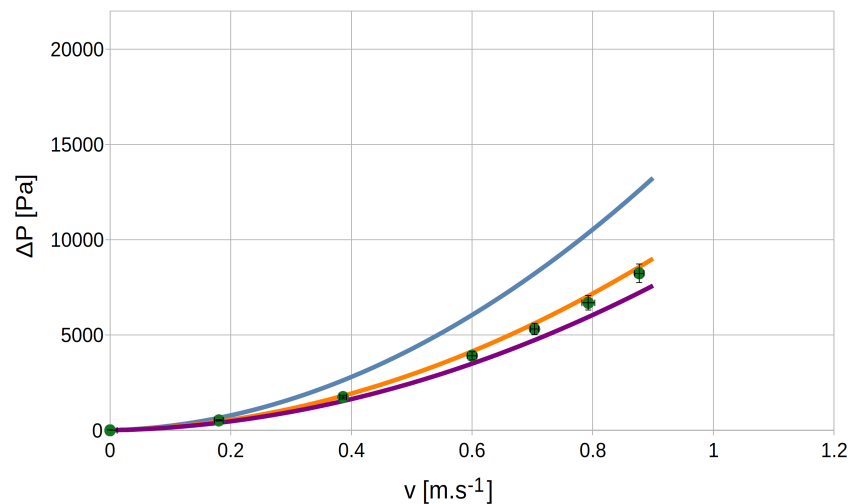


Figure 14. Comparison between the global pressure losses calculated from the final formula and measured from the experimental measurements with the fibrous porous surface 'TV Extra' depending on the inlet velocity.

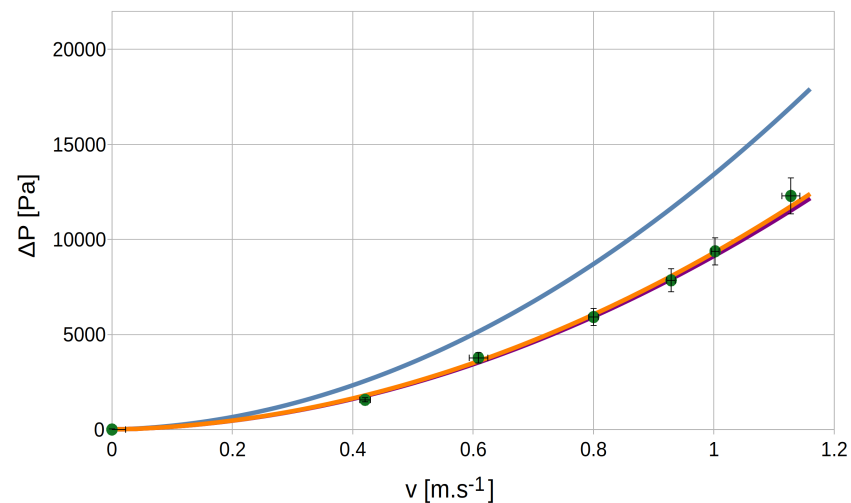


(a) 'TV' foam and 10 mm bars spacing

Figure 15. Cont.



(b) 'TV' foam and 15 mm bars spacing



(c) 'TV' foam and 24 mm bars spacing

Figure 15. Comparison of the global pressure losses for the fibrous porous surface 'TV' depending on the inlet velocity, including experimental results and pressure losses calculated by the analytical formula (Equation (11)) with the three approaches.

4. Discussion and Conclusions

This study considered the evolution of pressure losses for different configurations of a two-stage association composed of a porous fibrous medium in front of a bar rack. The global evolution of the pressure losses due to the single bar rack was found to depend on the square of the velocity according to the theory. For the porous media alone, the losses follow the Darcy–Forchheimer expression. By implementing the two stages together, it has been found that the resulting pressure losses needed a specific formulation. To understand the interdependence of these stages, various pressure loss combination models have been employed, comprising both series and interlaced approaches. A novel approach has been developed for the combination of pressure losses, taking into account the increased velocity in the porous media resulting from the presence of the bar rack immediately downstream. The proposed formulation employs an additional thickness factor to regulate the transitional velocity within the porous foam. The support simulations have facilitated the understanding of the topology of the flow passing through porous media. They have allowed the determination of the thickness factor for the porous fibrous foam. They also assisted in determining the characteristics of the porous foam surfaces

through readjustment. The developed formulae produce accurate results when applied to the examined cases. The final formula and the thickness factor may be further developed to adapt to more porous media types and other multi-stage obstacle associations.

By considering the combination of multiple stages beyond simple series or interlaced associations, this work contributes to the understanding and estimation of pressure losses through complex configurations in which the successive stages are mutually influenced. In addition to the current application of integral clogging, further developments are underway to model non-homogeneous clogging on inclined bar racks.

Author Contributions: Conceptualization: G.B., L.C., Y.L.G. and L.D.; methodology: G.B., L.C. and L.D.; software: G.B. and L.C.; validation: G.B., L.C., Y.L.G., X.C., C.B. and L.D.; data curation: G.B.; writing—original draft preparation: G.B.; writing—review and editing: G.B., L.C., Y.L.G., C.B. and L.D.; funding acquisition: L.C., Y.L.G., X.C., C.B. and L.D. All authors have read and agreed to the published version of the manuscript.

Funding: This work was funded by France Hydro Electricité (Paris, France) and the National Association for Technological Research (ANRT)—CIFRE N°2021/1425.

Data Availability Statement: The data presented in this study are available on request from the corresponding author. The data are not publicly available due to privacy or ethical restrictions.

Acknowledgments: This work was carried out in collaboration with the PPRIME Institute, Université de Poitiers (Poitiers, France), France Hydro Electricité (Paris, France), and the SIAME Laboratory, Université de Pau et des Pays de l'Adour (Pau, France). The experiments were carried out on the Plateform Hydrodynamique Environnementale (pHE). Their support and help are greatly appreciated.

Conflicts of Interest: The authors declare no conflicts of interest.

Notations

The following notations are used in this manuscript:

A_i	form coefficient of a bar [-]
E_{max}	maximum relative error [%]
E_{mean}	mean of the relative error [%]
ISS	International Space Station
K_{foam}	factor depending on foam characteristics [-]
K	permeability coefficient [m^2]
Re_b	bar Reynolds number [-]
TI	turbulent intensity [-]
b	bar width [m]
e	bar spacing [m]
f_t	thickness factor [-]
k	turbulent kinetic energy [$m^2 \cdot s^{-2}$]
o_b	bar rack obstruction ratio [-]
p	bar depth [m]
p_{static}	static pressure [Pa]
v	inlet water velocity [$m \cdot s^{-1}$]
v_x	water velocity in the x -direction [$m \cdot s^{-1}$]
v_y	water velocity in the y -direction [$m \cdot s^{-1}$]
v_a	water velocity between bars [$m \cdot s^{-1}$]
v_t	transition water velocity in the porous foam [$m \cdot s^{-1}$]
y^+	dimensionless wall distance [-]
ΔP	global pressure difference [Pa]
ΔP_{foam}	foam pressure difference [Pa]
ΔP_{grid}	bar rack pressure difference [Pa]
Δx	porous foam thickness [m]
α	Ergün coefficient [-]
β	Inclination angle of the bar rack [°]

ϵ	dissipation of kinetic energy [$\text{m}^2 \cdot \text{s}^{-3}$]
ζ	pressure loss coefficient [-]
μ	dynamic viscosity [$\text{Pa} \cdot \text{s}$]
ν	kinetic viscosity [$\text{m}^2 \cdot \text{s}^{-1}$]
ν_t	turbulent viscosity [$\text{m}^2 \cdot \text{s}^{-1}$]
ρ	water density [$\text{kg} \cdot \text{m}^{-3}$]
ω	turbulent specific dissipation rate [s^{-1}]

References

- Idel'cik, I.; Meury, M. *Mémento des Pertes de Charge: Coefficients de Pertes de Charge Singulières et de Pertes de Charge par Frottement*/I.E. Idel'cik; Traduit du Russe par Madame M. Meury; Collection du Centre de Recherches et d'essais de Chatou, Eyrolles: Paris, France, 1969.
- Blevins, R. *Applied Fluid Dynamics Handbook*; Krieger Pub.: Malabar, FL, USA, 2003; ISBN 1-57524-182-X.
- Rodriguez, F. The analogy between fluid flow and electric circuitry. *Chem. Eng. Educ. Fla. Online J.* **1979**, *13*, 96–98.
- Lemkecher, F.; Chatellier, L.; Courret, D.; David, L. Contribution of Different Elements of Inclined Trash Racks to Head Losses Modeling. *Water* **2020**, *12*, 966. [[CrossRef](#)]
- Xiong, W.; Kalkühler, K.; Merzkirch, W. Velocity and turbulence measurements downstream of flow conditioners. *Flow Meas. Instrum.* **2003**, *14*, 249–260. [[CrossRef](#)]
- Cho, H.H.; Rhee, D.H. Local heat/mass transfer measurement on the effusion plate in impingement/effusion cooling systems. *J. Turbomach.* **2000**, *123*, 601–608. [[CrossRef](#)]
- La Rosa, D.M.; Rossi, M.M.A.; Ferrarese, G.; Malavasi, S. On the pressure losses through multistage perforated plates. *J. Fluids Eng.* **2021**, *143*, 061205. [[CrossRef](#)]
- La Rosa, D.M.; Rossi, M.M.A.; Ferrarese, G.; Malavasi, S. Numerical investigation of parameters affecting energy losses in multi-stage perforated plates. *J. Fluids Eng.* **2023**, *145*, 091204. [[CrossRef](#)]
- Qian, J.Y.; Hou, C.W.; Wu, J.Y.; Gao, Z.X.; Jin, Z.J. Aerodynamics analysis of superheated steam flow through multi-stage perforated plates. *Int. J. Heat Mass Transf.* **2019**, *141*, 48–57. [[CrossRef](#)]
- Haimin, W.; Shujuan, X.; Qingyi, S.; Caimin, Z.; Hao, L.; Eryun, C. Experiment study on pressure drop of a multistage letdown orifice tube. *Nucl. Eng. Des.* **2013**, *265*, 633–638. [[CrossRef](#)]
- Kang, D.H.; Kim, N.K.; Kang, H.W. Electrostatic Charge Retention in PVDF Nanofiber-Nylon Mesh Multilayer Structure for Effective Fine Particulate Matter Filtration for Face Masks. *Polymers* **2021**, *13*, 3235. [[CrossRef](#)]
- Agui, J.H.; Green, R.D.; Vijayakumar, R. Development of a Multi-Stage Filter System for Cabin Ventilation Systems on the ISS and Future Deep Space Missions. In Proceedings of the International Conference on Environmental Systems (ICES 2018), Albuquerque, NM, USA, 8–12 July 2018.
- Walczak, N.; Walczak, Z.; Nieć, J. Influence of Debris on Water Intake Gratings in Small Hydroelectric Plants: An Experimental Study on Hydraulic Parameters. *Energies* **2021**, *14*, 3248. [[CrossRef](#)]
- Walczak, N. Operational Evaluation of a Small Hydropower Plant in the Context of Sustainable Development. *Water* **2018**, *10*, 1114. [[CrossRef](#)]
- Yan, T.; Qiu, B.; Yuan, J.; Qi, G. Experimental investigation on flow of trash rack blockage in front of pumping station. *J. Hydraul. Res.* **2023**, *61*, 775–787. [[CrossRef](#)]
- Schalko, I.; Ruiz-Villanueva, V.; Maager, F.; Weitbrecht, V. Wood Retention at Inclined Bar Screens: Effect of Wood Characteristics on Backwater Rise and Bedload Transport. *Water* **2021**, *13*, 2231. [[CrossRef](#)]
- Schalko, I.; Weitbrecht, V. Wood blockage and sediment transport at inclined bar screens. *J. Hydraul. Res.* **2021**, *60*, 164–172. [[CrossRef](#)]
- Zayed, M.; Farouk, E. Effect of blocked trash rack on open channel infrastructure. *Water Pract. Technol.* **2021**, *16*, 247–262. [[CrossRef](#)]
- Walczak, N.; Walczak, Z.; Nieć, J. Assessment of the Resistance Value of Trash Racks at a Small Hydropower Plant Operating at Low Temperature. *Energies* **2020**, *13*, 1775. [[CrossRef](#)]
- Gebre, S.; Timalisina, N.; Alfredsen, K. Some Aspects of Ice-Hydropower Interaction in a Changing Climate. *Energies* **2014**, *7*, 1641–1655. [[CrossRef](#)]
- Meusburger, H. *Energieverluste an Einlaufrechen von Flusskraftwerken*. Ph.D. Thesis, ETH, Zürich, Switzerland, 2002.
- Raynal, S.; Chatellier, L.; David, L.; Courret, D.; Larinier, M. Fish-friendly trashracks: Headloss formula and clogging effect for inclined racks. In Proceedings of the 2nd IAHR Europe Congress, Munich, Germany, 27–29 June 2012; p. 0. hal-04086634.
- Hribernik, A. Evaluation of Clogged Hydropower Plant Trash Rack Losses. *Stroj. Vestn. J. Mech. Eng.* **2020**, *66*, 142–152. [[CrossRef](#)]
- Dziubak, T. Experimental Testing of Filter Materials for Two-Stage Inlet Air Systems of Internal Combustion Engines. *Energies* **2024**, *17*, 2462. [[CrossRef](#)]
- Violeau, D.; EL Kadi Abderrezzak, K.; Buvat, C.; Gueguen, N.; Castro-Orgaz, O.; Cicero, G.M. Steady free-surface flow in vegetation debris pad clogging trash racks. *J. Hydraul. Res.* **2024**, *62*, 223–235. [[CrossRef](#)]

26. Grahn, A.; Krepper, E.; Alt, S.; Kästner, W. Implementation of a strainer model for calculating the pressure drop across beds of compressible, fibrous materials. *Nucl. Eng. Des.* **2008**, *238*, 2546–2553. [[CrossRef](#)]
27. Sotoodeh, K. Handling the pressure drop in strainers. *Mar. Syst. Ocean. Technol.* **2019**, *14*, 220–226. [[CrossRef](#)]
28. Raynal, S. Étude Expérimentale et Numérique des Grilles Ichtyocompatibles. Ph.D. Thesis, Université de Poitiers, Poitiers, France, 2013.
29. Raynal, S.; Chatellier, L.; David, L.; Courret, D.; Larinier, M. Numerical simulations of fish-friendly angled trashracks at model and real scale. In Proceedings of the 35th IAHR World Congress, Chengdu, China, 8–13 September 2013.
30. Raynal, S.; Dominique, C.; Ludovic, C.; Michel, L.; David, L. An experimental study on fish-friendly trashracks—Part 1. Inclined trashracks. *J. Hydraul. Res.* **2013**, *51*, 56–66. [[CrossRef](#)]

Disclaimer/Publisher’s Note: The statements, opinions and data contained in all publications are solely those of the individual author(s) and contributor(s) and not of MDPI and/or the editor(s). MDPI and/or the editor(s) disclaim responsibility for any injury to people or property resulting from any ideas, methods, instructions or products referred to in the content.